

Measurement of the properties of the 125 GeV Higgs boson with the CMS detector

João Varela¹

Laboratório de Instrumentação e Partículas

Av. Elias Garcia, 1000-149 Lisbon, Portugal

Deputy Spokesperson, CMS Experiment

E-mail: joao.varela@cern.ch

Abstract. The measurement of the properties of the recently discovered boson is central to the LHC physics program. In this contribution we review preliminary measurements of the properties of the new 125 GeV boson performed by the CMS experiment using the full proton-proton dataset collected in 2011-12 ($\sim 25 \text{ fb}^{-1}$). In the $H \rightarrow ZZ (4l)$ channel, a signal significance of 6.7σ is now observed. In the other high-resolution mode, $H \rightarrow \gamma\gamma$, updated results were obtained on the signal strength, $\mu = \sigma/\sigma_{\text{SM}}$, which is now measured to be $\sim 0.8 \pm 0.3$. The two high-resolution modes allowed independent determinations of the Higgs mass: $125.8 \pm 0.6 \text{ GeV}$, in $H \rightarrow ZZ (4l)$; and $125.4 \pm 0.8 \text{ GeV}$, in $H \rightarrow \gamma\gamma$. The four-lepton channel permitted tests of the spin-parity of the new boson. From these studies, the pure pseudoscalar hypothesis is excluded at 99.8% C.L. and, for the first time, simple spin 2 models are excluded with greater than 98.5% C.L. Significantly, strong evidence is seen in a fermionic decay mode of the Higgs for the first time, namely in the $H \rightarrow \tau\tau$ channel, which is reported with a significance of nearly 3σ . The new measurements of the spin-parity (J^P) assignments for this particle, coupled with the measured strength of the interaction of this particle with other particles, strongly indicates that the new particle is a Higgs boson, responsible for the Electroweak Symmetry Breaking. While all of these measurements are consistent with values predicted for a SM Higgs boson, they still fall far short of the requisite precision to rule out all BSM scenarios. Additional data from Run 2 of the LHC and HL-LHC will be needed to firmly establish this conclusion.

1. Introduction

The Higgs boson is the quantum of a scalar field that is postulated to give mass to W^+ , W^- and Z^0 bosons and to explain the masses of the fundamental quarks and leptons. It has been the target of searches at accelerators around the world for more than a quarter of a century. In the context of a Higgs boson search in proton-proton collisions at the Large Hadron Collider at CERN [1], the ATLAS and CMS experiments have observed a new particle with a statistical significance of five standard deviations using the first 10 fb^{-1} of data at 7 and 8 TeV [2,3].

The LHC has accelerated and collided beams of protons at energies of $\sqrt{s} = 7$ (8) TeV in 2011 (2012). The LHC peak luminosity in 2012 was approximately $7.7 \times 10^{33} \text{ cm}^{-2}\text{s}^{-1}$, achieved with 1368

¹ On behalf of the CMS Collaboration



proton bunches per beam at 50 ns separation with up to $\sim 1.5 \times 10^{11}$ protons per bunch squeezed to a transverse size of about 20 μm at the interaction point. At this luminosity each bunch-crossing yields on average 39 proton-proton (pp) collisions known as pileup.

The Standard Model Higgs production cross section increases with \sqrt{s} and decreases with m_H . At $\sqrt{s} = 8$ TeV and for $m_H = 125$ GeV, the probability of SM Higgs boson production per pp collision is $\sim 10^{-10}$. For every fb^{-1} of integrated luminosity about 20,000 SM Higgs bosons with mass 125 GeV are expected to be produced. The majority of these decay to final states that have large background, making identification difficult or impossible. CMS developed dedicated methods to exploit channels with lower decay fractions by selecting kinematical regions of the decay products where the signal-to-background ratio is sufficiently large to make the observation of a SM Higgs boson possible.

Following the observation of the new boson, the measurement of the properties of this new particle became central to the CMS physics program. In this contribution we review preliminary measurements of the properties of the new 125 GeV boson performed by the CMS experiment using the full pp dataset collected in 2011-12 ($\sim 25 \text{ fb}^{-1}$). Five main decay modes are studied involving bosons ($\gamma\gamma$, ZZ , W^+W^-) and the heaviest accessible fermions ($b\bar{b}$, $\tau^+\tau^-$).²

2. CMS detector

The CMS detector measures particles produced in high-energy proton-proton and heavy-ion collisions [4]. The central feature of the detector is a superconducting solenoid 13 m long, with an internal diameter of 6 m. Within its volume it generates a uniform 3.8 T magnetic field along the axis of the LHC beams. Within the field volume are a silicon pixel and strip tracker, a lead tungstate (PbWO_4) scintillating crystal electromagnetic calorimeter and a brass/scintillator hadron calorimeter. Muons are identified and measured in gas-ionization detectors embedded in the outer steel magnetic-flux-return yoke. The detector is subdivided into a cylindrical barrel part, and endcap disks on each side of the interaction point. Forward calorimeters complement the coverage provided by the barrel and endcap detectors. The CMS detector has a large angular acceptance, detecting particles over the full azimuthal range and with θ larger than 0.8 degrees, where θ is the polar angle relative to the beam axis.

The silicon tracker has 66M pixels and 9.3M strips in 13 (11) layers in the central (forward) regions for $> 99\%$ tracking efficiency and 1.5-3% p_T resolution at 100 GeV. Decay vertices are reconstructed with high efficiency and precision. Electrons and photons are detected in ECAL's 75,848 PbWO_4 crystals and measured with a precision of $\sim 1\%$ for the photons and electrons considered for the results presented here. Similarly, the muon system has transverse momentum (p_T) resolution better than 1% for the muons used in these analysis.

CMS uses a two-level online trigger system to reduce the event rate from the bunch crossing frequency to ~ 500 Hz of events recorded in disk by selecting events with leptons, photons, jets, high energy (ΣE_T), missing transverse energy (E_T^{miss}) or combinations of these features. Level 1 uses custom electronics to analyze calorimeter and muon information and has an output rate ≤ 95 kHz. The High Level Trigger uses 13,000 processors to study data from all sub-detectors. Billions of events are recorded each year and sent to computing centers around the world for reconstruction and analysis.

3. Properties of the 125 GeV boson

In 2011 CMS collected 5.1 fb^{-1} of data at 7 TeV. The LHC collision energy was raised to 8 TeV in 2012, leading to $\sim 25\%$ increase in SM Higgs boson production in the low mass region. By the end of 2012, CMS collected 19.6 fb^{-1} data at $\sqrt{s} = 8$ TeV.

At the LHC the SM Higgs boson is produced mainly through gluon-gluon fusion. Two additional important production processes are vector boson fusion (VBF) and associated production (VH), where

² We do not show particle charges in the remainder of the text.

$V = W$ or Z . The latter two modes have better signal-to-background (S/B), but have much lower rates [5–9]. VBF events involve high-energy forward jets that can help identify this production mode.

Large samples of simulated events are used to refine the analysis techniques, estimate backgrounds and predict the expected significance for the observation of new particles [10–13]. Whenever possible backgrounds are derived from data control samples.

3.1 Decay mode $H \rightarrow \gamma\gamma$

The $H \rightarrow \gamma\gamma$ decay channel provides a clean final state topology which allows the mass to be reconstructed with high precision. At mass $m_H = 125$ GeV, $H \rightarrow \gamma\gamma$ is one of the most sensitive channels for the Higgs measurement despite its low branching fraction of the order of $\sim 0.2\%$ [14].

The search results are presented for an analysis that uses Multi-Variate-Analysis (MVA) techniques [16, 17] both for photon identification and event classification, and extracts the signal from the background using a fit to the diphoton mass spectrum [15]. To achieve the best sensitivity to a Standard Model Higgs boson decaying to two photons, the events are separated into classes. The classes have successively looser quality criteria as determined by mass resolution, photon kinematics, absence/presence of conversions, isolation etc. Unconverted photons tend to have higher quality and higher S/B for SM Higgs, particularly for large $p_T(\gamma\gamma)$. Additional event classes are defined to identify the events from specific production mechanisms, selecting events based on the presence of additional objects in the final state. The presence of two forward jets selects events produced by the vector boson fusion (VBF) production mechanism while events with a muon, an electron, or missing transverse energy (E_T^{miss}) target production in association with a vector boson (VH).

The analysis searches for a localized excess of diphoton events over a smoothly falling background due to prompt diphoton production and to events with at least one jet misidentified as photon. Energy resolution and scale are thus the critical parameters. An *in-situ* ECAL calibration uses $\pi^0, \eta^0 \rightarrow \gamma\gamma$ decays and electrons from W and Z decays. Radiation causes a small loss of transparency in ECAL crystals. This is monitored in real-time by a laser system to obtain corrections enabling a response uniformity of $\pm 0.2\%$ as verified by the E/p ratio for electrons from $W \rightarrow e\nu$ decays. $Z \rightarrow ee$ data are used for the final energy resolutions and scales.

The diphoton mass resolution is not strongly affected by angular resolution of the photon trajectories provided that the interaction point is known to better than ~ 1 cm. This can be a challenge in a high pileup environment, particularly since photons cannot be tracked unless they convert to an e^+e^- pair. To find the correct vertex, a variety of vertex-related information such as Σp_T^2 and overall p_T balance of tracks relative to the momentum of the $\gamma\gamma$ system is used in a multivariate analysis based on boosted decision trees. Information from conversions is also used when it is available. Boosted decision trees are also used to identify photons and to extract their energies and uncertainties. The full set of selection criteria are provided in ref. [15] for the data considered here.

The description of the Higgs boson signal is obtained from MC simulation using the next-to-leading order (NLO) matrix-element generator POWHEG [18, 19] interfaced with PYTHIA [20]. For the dominant gluon fusion process events have been reweighted to reproduce the NNLL+NNLO distributions computed by the HQT program [21, 22]. The SM Higgs boson cross sections and branching fractions used are taken from ref. [23]. The background estimation is entirely data driven. The background models are obtained by fitting the observed diphoton mass distributions in each of the event classes over the range 100–180 GeV. Polynomials of orders from 2 to 5 are used to model the background distributions in the various categories. By design, the choice of the background model induces a bias on the fitted signal strength less than five times the statistical uncertainty on the background [24]. Therefore the systematic associated to the background shape can be safely neglected.

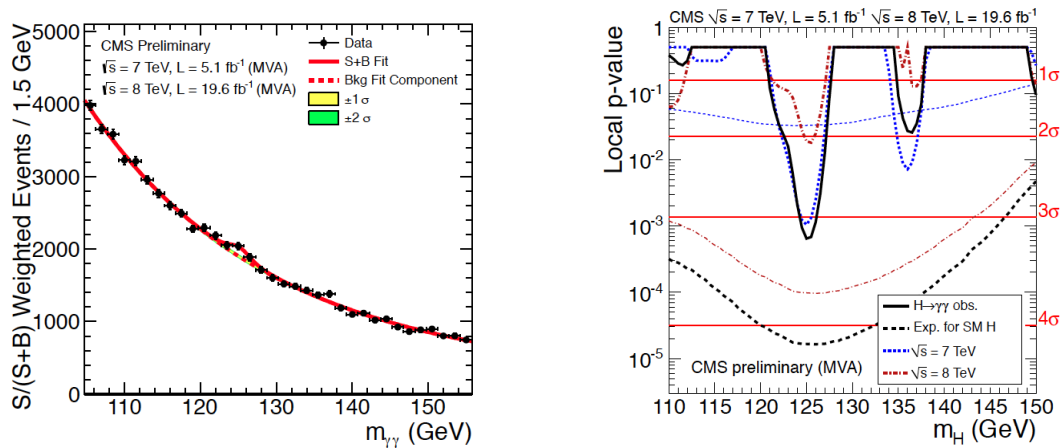


Figure 1. Left: Combination of $m_{\gamma\gamma}$ event class distributions weighted by $S/(S+B)$. Solid red lines show fits to $S+B$ assuming a 125 GeV SM Higgs. Dashed red lines show background-only with 1 and 2 σ bands in yellow and green, respectively. Right: The observed probability (local p-value) as a function of m_H for the background to fluctuate to the excess observed.

Figure 1 shows the mass spectrum where the event classes are weighted by $S/(S+B)$ and combined. An excess of events is seen at 125 GeV that is consistent with expectations for a SM Higgs. The background mostly involves SM processes producing two real photons. A smaller fraction involves a real photon and a fake photon from a misidentified jet. The magnitude of the excess above the background for all categories combined has a significance of 3.2 σ relative to the background-only hypothesis, where a local significance of 4.2 σ is expected from a Standard Model Higgs boson. Consistent excesses are present in 2011 and 2012 data. The best fit signal strength corresponding to the largest signal like fluctuation at 125 GeV is $\sigma/\sigma_{\text{SM}} = 0.78^{+0.28}_{-0.26}$.

The calibration of the energy scale is established with reference to the known Z boson mass. The two main sources of systematic uncertainty are the imperfect simulation of the detector response to electrons/photons and the mis-modeling of the extrapolation from the Z to the Higgs energy scale. Figure 2 shows the 2D 68% and 95% CL contours for the signal strength and the mass of the observed particle (left) and the scan of the negative-log-likelihood as a function of the mass (right). From the later, the mass of the observed boson is measured to be $125.4 \pm 0.5(\text{stat.}) \pm 0.6(\text{syst.})$ GeV.

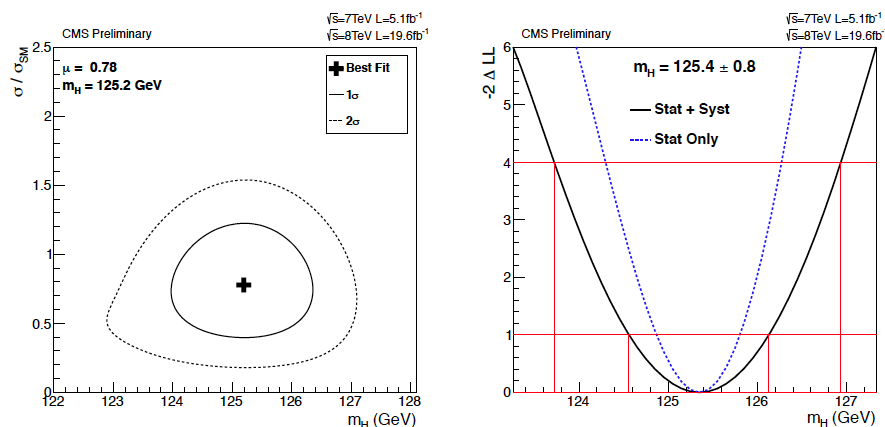


Figure 2. Left: The 2D 68% confidence level region for the signal strength and the mass of the observed particle. Right: The scan of the negative-log-likelihood as a function of the mass.

The four main Higgs boson production mechanisms can be associated with either top-quark couplings (gluon fusion and ttH) or vector boson couplings (VBF and VH). Figure 3 shows the 68% and 95% CL contours for the signal strength modifiers associated with the gluon fusion plus ttH and for VBF plus VH production mechanisms. The observed values are consistent with the expectations from the production of a SM Higgs boson.

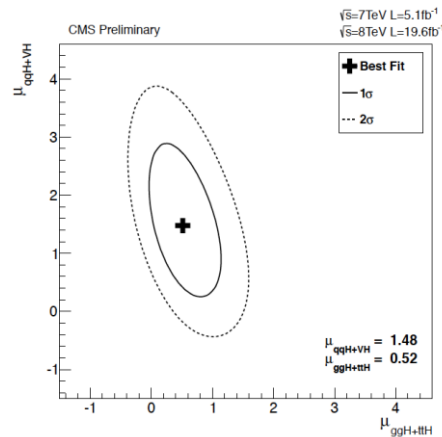


Figure 3. The 68% and 95% CL intervals for the signal strength modifiers associated with the gluon fusion plus ttH and for VBF plus VH production mechanisms. The cross indicates the best-fit value.

3.2 Decay mode $H \rightarrow ZZ^* \rightarrow 4l$

The branching ratio $B(H \rightarrow ZZ^*)$ is $\sim 2.6\%$ for a 125 GeV Higgs where there is at least one off-shell Z. The decays $Z \rightarrow ll$ where $l = e, \mu$ have smallest backgrounds, producing $2e2\mu$, $4e$ and 4μ final states. In this contribution, we present an update of the properties of the new boson measured in this channel using the whole 2011-12 dataset. The properties reported here are the mass, the signal strength relative to the expectation for the SM Higgs boson and the spin-parity quantum numbers. A more complete account of the results can be found in [25, 31].

Collision events are selected by the trigger system that requires the presence of a pair of electrons or a pair of muons, or a triplet of electrons. The minimal momenta of the first and second lepton are 17 and 8 GeV, respectively, for the double lepton triggers, while they are 15, 8 and 5 GeV for the triple electron trigger. The trigger efficiency within the acceptance of this analysis is greater than 98% for a Higgs boson signal with $m_H > 120$ GeV.

Offline selection cuts go down to 5 (7) GeV for μ (e) in $|\eta| < 2.4$ (2.5). We require the presence of four isolated leptons that originate from the same interaction vertex. Both Z boson candidates are required to decay to two same-flavor leptons of opposite charge and the invariant mass of the dileptons produced in the Z boson decays must be in the range 40–120 GeV for the heavier of the two, and 12–120 GeV for the lighter one.

The invariant mass of the ZZ system can be reconstructed and measured with good accuracy in CMS from the four-lepton momenta. Hence, the presence of a Higgs boson in the data should manifest itself as a peak in the ZZ invariant mass spectrum in the presence of a small continuum background. SM background processes include irreducible, non-resonant ZZ^* production which is estimated via Monte Carlo (MC). Other backgrounds such as individual Z bosons produced in association with heavy-flavor jets and tt production are estimated from data.

MC samples for the SM Higgs boson signal and for background processes are used to optimize the event selection and to evaluate the acceptance and systematic uncertainties. The Higgs boson signals are generated with POWHEG [26] at next-to-leading order (NLO). Signal samples with alternative spin-parity scenarios are generated with JHUGen [27] at Leading Order (LO). At low mass,

the analysis is carried out in the framework of the narrow-width approximation, describing the Higgs lineshape with a Breit-Wigner distribution. At high mass the lineshape is corrected to match the results presented in [28–30]. Events at generator level are reweighted according to the total cross section $\sigma(pp \rightarrow H)$ containing contributions up to next-to-next-to-leading order (NNLO). The total cross section is scaled by the branching fraction $B(H \rightarrow 4l)$ calculated with PROPHECY4F. These higher order corrections are described in the references quoted in [31]. The SM background contribution from ZZ production via qq is generated at NLO with POWHEG, while other diboson processes (WW, WZ) are generated with MADGRAPH [32] with cross sections rescaled to NLO predictions. The $gg \rightarrow ZZ$ contribution is generated with GG2ZZ [33].

The mass spectrum for selected events is shown in Figure 4. A lepton can radiate a photon at an early stage, potentially leading to an underestimate of its energy if this is not taken into account. Photons consistent with final state radiation are thus included in the lepton energy calculation where appropriate. Figure 4 displays a statistically significant peak near 125 GeV confirming the results reported in [2]. There is also a clear Z peak at 91 GeV from $Z \rightarrow 4l$ where one lepton pair comes from the conversion of an energetic virtual photon.

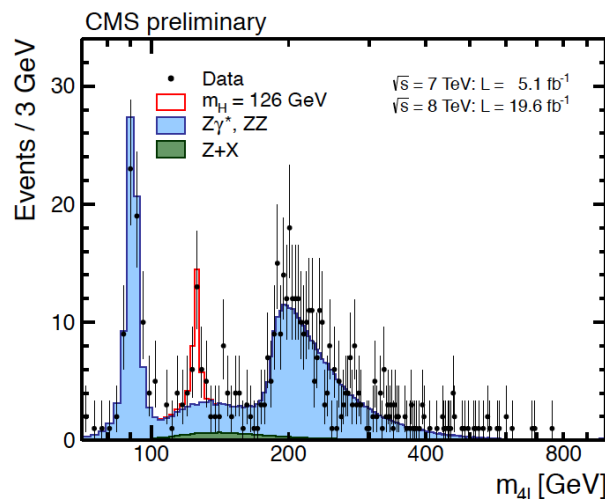


Figure 4. Distribution of invariant mass for $4e$, 4μ and $2e2\mu$ with expectations for background and 126 GeV SM Higgs indicated.

Five angles and the invariant masses of the lepton pairs fully describe the kinematics of the decay process at a given mass of the four-lepton system. These observables provide significant discriminating power between signal and background. We use a matrix element likelihood approach [2] to construct a kinematic discriminant K_D based on the probability ratio of the signal and background hypotheses, where the leading-order matrix elements define the probabilities for each value of m_{4l} . Several choices of matrix elements have been studied for signal and background, including analytical parameterization [27,35,35], JHUGEN [27, 34], MCFM [36–38] implemented within the MELA framework [2] and MADGRAPH [32] implemented within the MEKD framework [39]. Different matrix elements were found to provide nearly identical performance. MVA techniques such as boosted decision trees or Bayesian neural networks were also investigated and provided similar results as the matrix element approaches. The distributions of the kinematic discriminant K_D versus the four-lepton reconstructed mass m_{4l} are shown for the selected events and compared to expectations in Fig. 5. The distribution of events is seen to agree well with the SM expectations in the high mass range, while the accumulation of events seen at high K_D is consistent with the expected signal for $m_H = 126$ GeV.

The local p-values, representing the significance of local excesses relative to the background expectation, are shown as a function of m_H in Fig. 6. The minimum is reached around $m_{4l} = 125$ GeV,

and corresponds to a local significance of 6.7σ (for an expectation of 7.1σ). This constitutes an observation of the new boson in the four-leptons channel alone.

The signal strength μ , relative to the expectation for the SM Higgs boson, is measured to be $\mu=0.91^{+0.30}_{-0.24}$ at 125.8 GeV. Using simulation it is found that the distribution of the kinematic discriminant K_D for the signal at a mass around $m_H = 126$ GeV is similar for a scalar, pseudo-scalar, vector, pseudo-vector or a spin-two resonance with the minimal couplings [27]. Therefore the results presented are nearly model-independent in the low-mass region.

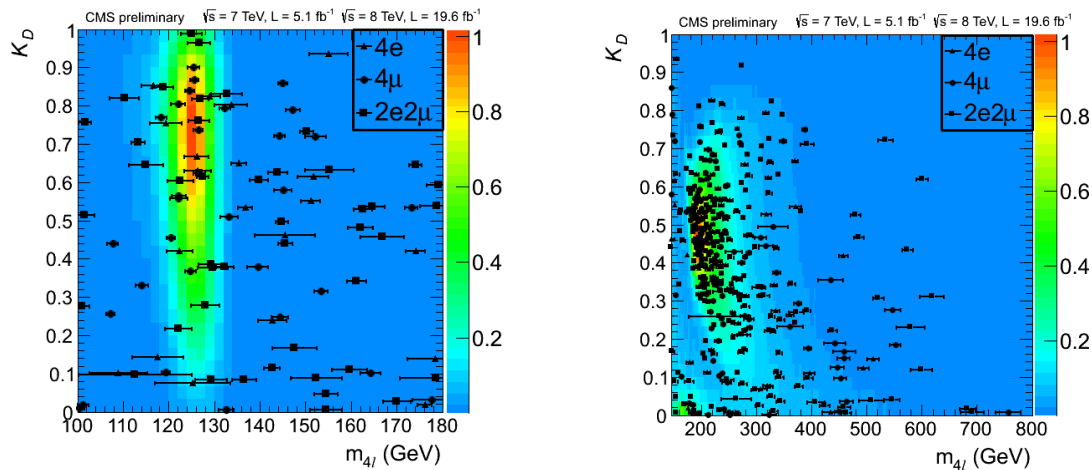


Figure 5. Distribution of the kinematic discriminant K_D versus the four-lepton reconstructed mass m_{4l} in the low-mass range [100-180] GeV (left) and in the high-mass range [180-800] GeV (right). The points representing the individual events are shown together with their reconstructed mass uncertainties. The contours represent the signal expectation for $m_H = 126$ GeV (left) and the SM background expectation (right).

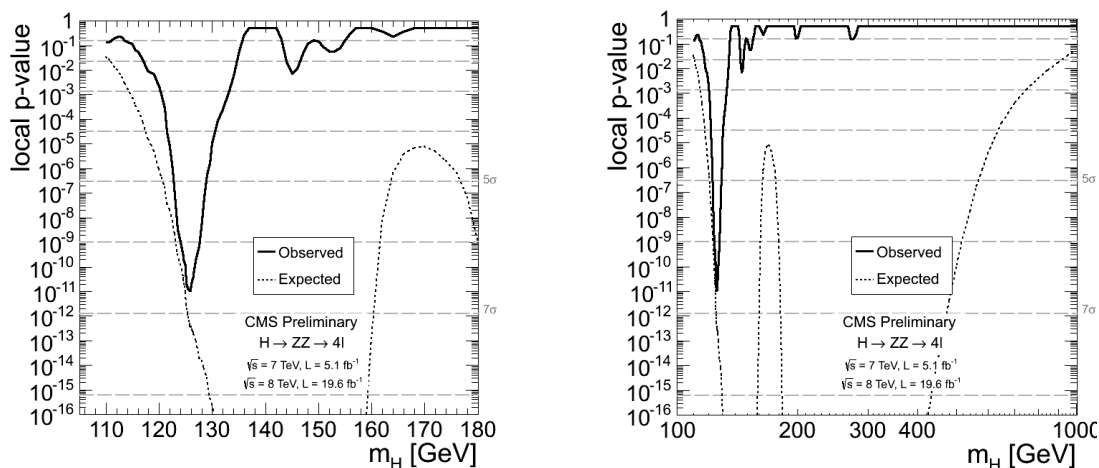


Figure 6. Significance of the local excess with respect to the standard model background expectation as a function of the Higgs boson mass for inclusive analysis. The results are shown for the full data sample in the range [110-180] GeV (left) and [110-1000] GeV (right) for the sum of the $4e$, 4μ , and $2e2\mu$ channels.

The mass measurement of the new resonance is performed with a three-dimensional fit using for each event the four-lepton invariant mass, the associated per-event mass error, and the kinematic discriminant. Figure 7 (left) shows the one-dimensional likelihood scan versus the Higgs boson mass.

The resulting fit gives $m_H = 125.8 \pm 0.5(\text{stat.}) \pm 0.2(\text{syst.})$ GeV. The systematic uncertainty accounts for the effect of the lepton momentum scale and resolution.

Categorization of events according to the number of jets and the utilization of variables sensitive to vector boson fusion are used to disentangle the production mechanisms of the observed new state. The production mechanisms are split into two categories depending on whether the production is induced by vector bosons (VBF, ZH, WH) or fermions (gluon fusion loop with quarks, ttH). Two respective signal strength modifiers (μ_F , μ_V) are introduced as scale factors to the SM expected cross section. The result of a two dimensional fit for the two signal strength modifiers assuming a mass hypothesis of $m_H=125.8$ GeV is shown in figure 7 (right). The measured values are consistent with the expectations from the production of a SM Higgs boson.

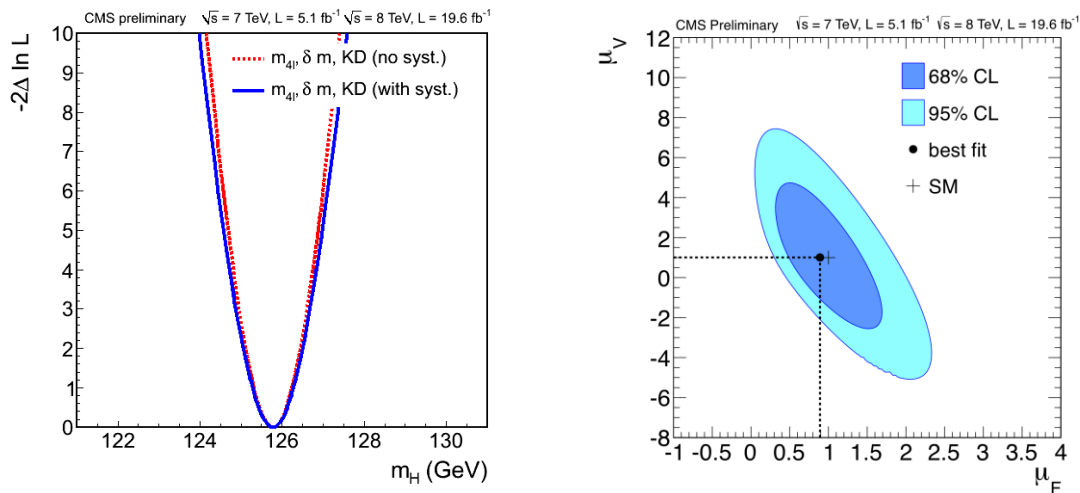


Figure 7. Left: One-dimensional likelihood scan versus the Higgs boson mass in the channel $H \rightarrow ZZ^* \rightarrow 4l$. Right: Likelihood contours on the signal strength modifiers associated with fermions (μ_F) and vector bosons (μ_V) shown at 68% and 95% CL.

The kinematics of the new boson decay to the $ZZ^*(4l)$ final state is sensitive to its spin and properties [27, 34]. We use this fact to determine its spin-parity following a methodology with a kinematic discriminant similar to the one used before but instead of the signal-to-background probability ratio we construct the probability ratio for two signal hypotheses. The discriminant for signal hypothesis testing is constructed as $D_{JP} = P_{SM} / (P_{SM} + P_{JP})$, where P_{SM} is the probability distribution for the SM Higgs boson hypothesis, and P_{JP} is the probability for an alternative model. The second observable is $D_{bkg} = P_{sig} / (P_{sig} + P_{bkg})$, where the probabilities P_{bkg} and P_{sig} also include the m_{4l} parameterizations of background and signal with $m_H = 126$ GeV. Simulation studies showed that the D_{bkg} distributions are very similar between the SM and alternative hypotheses but differ significantly from background.

The separation of the SM Higgs boson model from the pseudoscalar (0^-) or minimal coupling spin-2 resonance produced in gluon fusion ($2_{m_{gg}}^+$) has been presented by CMS [25], with data strongly disfavoring the pure pseudoscalar hypothesis. We present here additional tests of spin-parity hypotheses and consider the models $J^P = 0^+, 0_h^+, 0^-, 2_{m_{gg}}^+, 2_{m_{qq}}^+, 1^-, 1^+$, respectively the SM scalar, scalar with higher dimension operators, pseudoscalar, minimal coupling spin-2 resonance produced in gluon fusion and produced in quark-antiquark annihilation, exotic vector, and exotic pseudovector. In Figure 8 the D_{JP} distributions are shown in the mass range 106 to 141 GeV used to perform this measurement, for data and simulation.

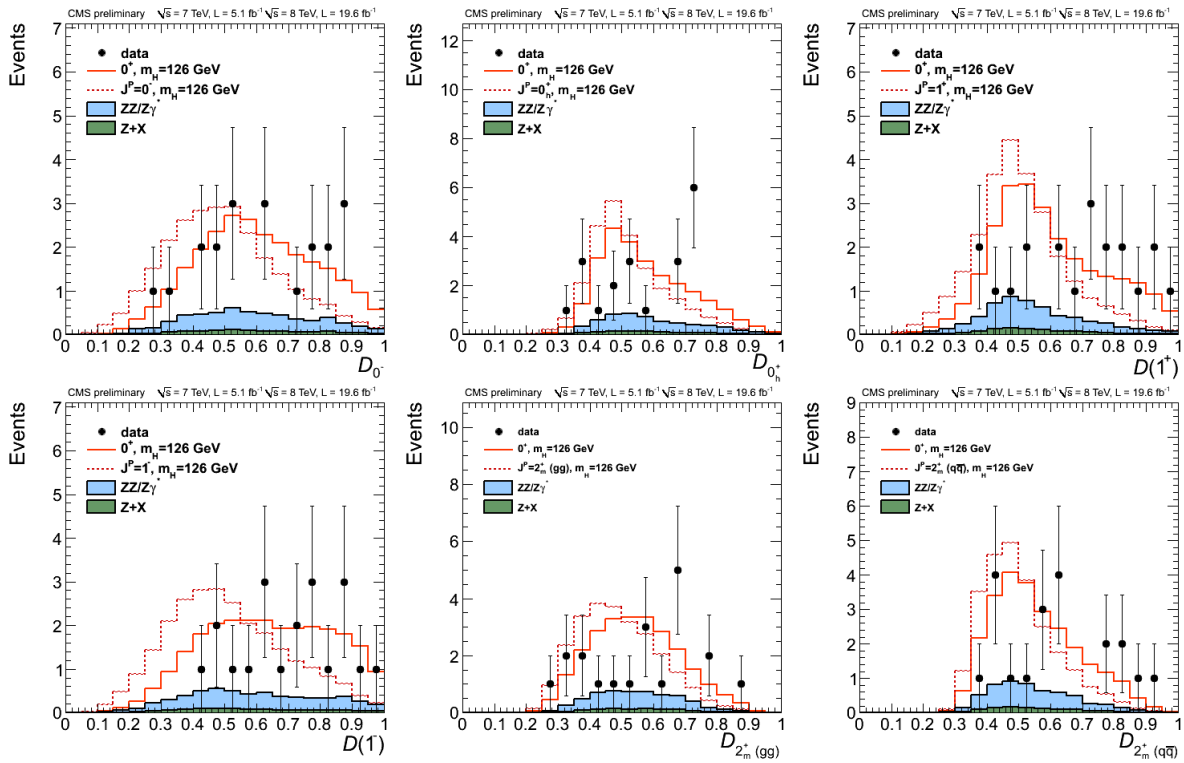
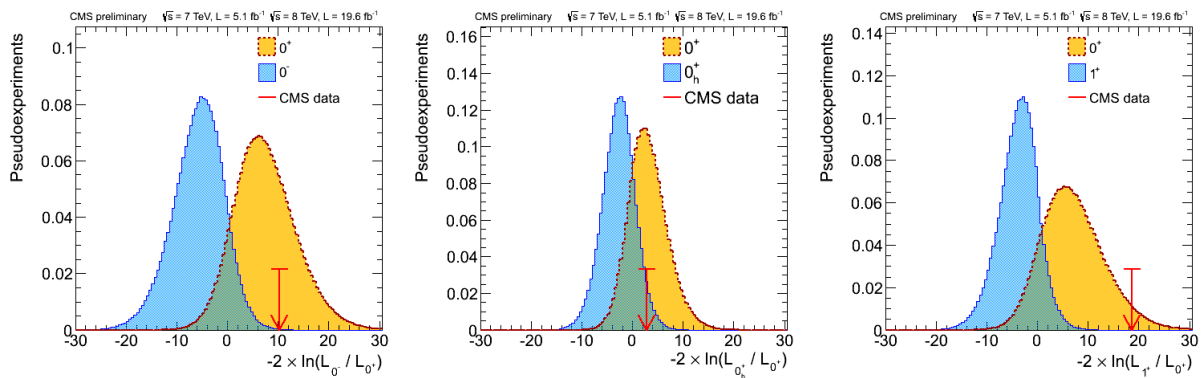


Figure 8. Distributions of D_{JP} with a requirement $D_{bkg} > 0.5$, in data (points with error bars) and expectations for background and signal. The six alternative signal hypotheses described in the text are tested.

A likelihood fit of the ensemble of selected events to the expected 2D distributions (D_{JP} , D_{bkg}) is performed with data and simulated samples, allowing the signal rates to float independently for each signal type. The distribution of the likelihood ratio $q = -2\ln(\mathcal{L}_P/\mathcal{L}_{SM})$ is obtained with generated samples of background and signal of seven types (SM 0^+ and six J^P) for $m_H=126$ GeV. The expected and observed values of q are shown in Figure 9 and the results are summarized in Table 1. We define a CL_S criterion as the ratio of the probabilities to observe, under the J^P and the 0^+ hypotheses, a value of the test statistics q equal or larger than the one in the data. The data disfavors the alternative hypotheses J^P with a CL_S value in the range 0.1–10%.



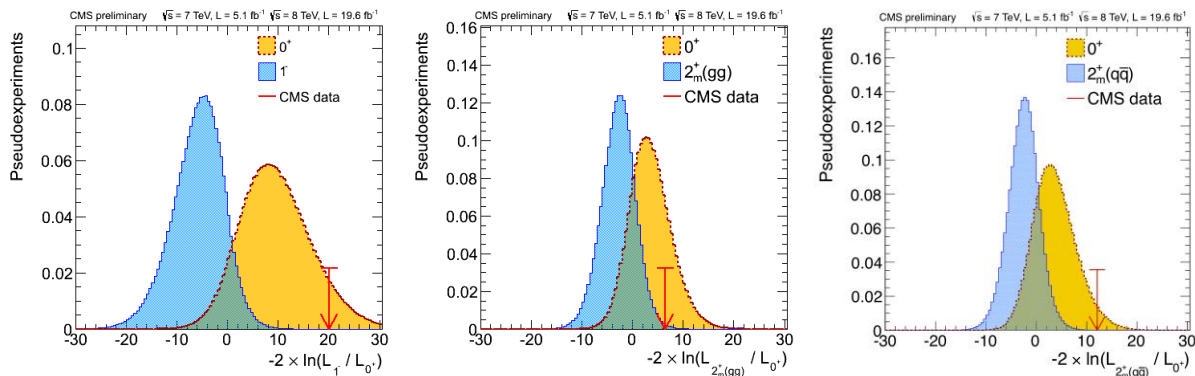


Figure 9. Distributions of $q = -2\ln(\mathcal{L}IP/\mathcal{L}SM)$ for two signal types (0^+ represented by the yellow histogram and alternative J^P hypothesis by the blue histogram) for $m_H=126$ GeV obtained with a large number of generated pseudo experiments. The arrow indicates the value observed in data. Six alternative hypotheses, described in the main text, are evaluated.

Table 1. List of models used in spin-parity analysis. The expected separation is quoted for two scenarios, when the signal strength is pre-determined from the fit to data and when events are generated with SM expectation for the signal yield ($\mu = 1$). The observed separation quotes the difference between the observation and the expected average of the 0^+ model or the J^P model expressed in standard deviations, and corresponds to the scenario where the signal strength is pre-determined from the fit to data. The last column quotes CLs criterion for the J^P model.

J^P	production	comment	expect ($\mu=1$)	obs. 0^+	obs. J^P	CLs
0^-	$gg \rightarrow X$	pseudoscalar	2.6σ (2.8σ)	0.5σ	3.3σ	0.16%
0^+_{h}	$gg \rightarrow X$	higher dim operators	1.7σ (1.8σ)	0.0σ	1.7σ	8.1%
$2^+_{\text{m}gg}$	$gg \rightarrow X$	minimal couplings	1.8σ (1.9σ)	0.8σ	2.7σ	1.5%
$2^+_{\text{m}qq}$	$qq \rightarrow X$	minimal couplings	1.7σ (1.9σ)	1.8σ	4.0σ	<0.1%
1^-	$qq \rightarrow X$	exotic vector	2.8σ (3.1σ)	1.4σ	$>4.0\sigma$	<0.1%
1^+	$qq \rightarrow X$	exotic pseudovector	2.3σ (2.6σ)	1.7σ	$>4.0\sigma$	<0.1%

3.3 Decay mode $H \rightarrow WW$

For $H \rightarrow WW$, the most sensitive final states contain two opposite-sign leptons (ee , $e\mu$ or $\mu\mu$) and significant $E_{\text{T}}^{\text{miss}}$ due to the undetected neutrinos. In contrast to the $\gamma\gamma$ and ZZ modes the mass cannot be reconstructed precisely. The signal is therefore expected to appear as an excess over background that extends over a broad mass range. Multivariate analysis techniques are used to optimize the sensitivity to signal. Events are categorized by lepton flavor content and jet multiplicity with different backgrounds and sensitivities. Jet identification and $E_{\text{T}}^{\text{miss}}$ require some care in a high pileup environment where energy deposits from multiple pp collisions can become intertwined. Pileup effects are largely neutralized by associating charged particles to their correct interaction vertices and by means of MVA techniques that use jet shape variables to separate real jets from clusters of pileup energy deposits. The final impact of pileup on the correct accounting of events with zero additional jets is negligible, as seen in Figure 10.

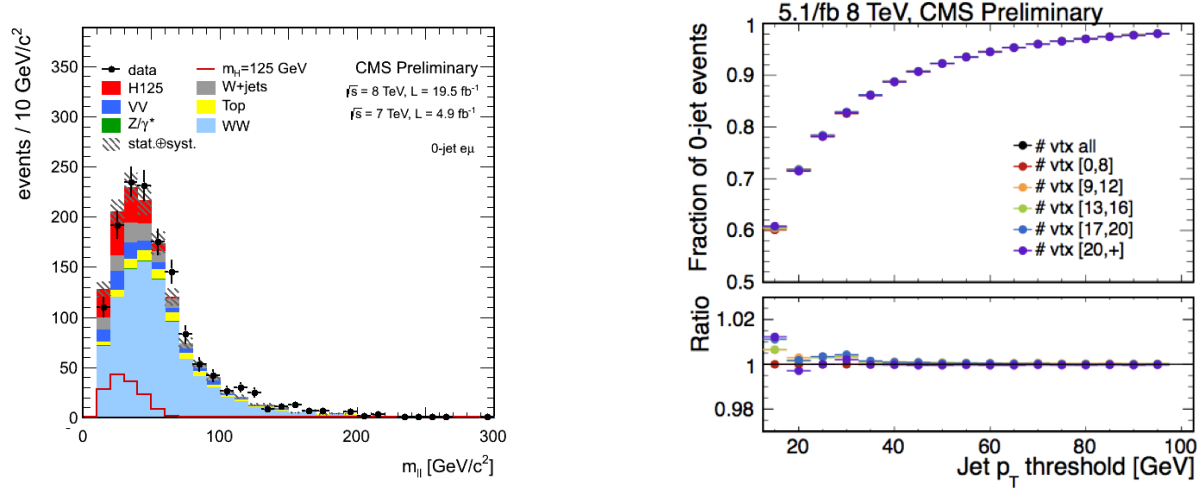


Figure 10. Left: Invariant mass of lepton pairs for the zero-jet $e\mu$ category in the search for $H \rightarrow WW$. The 125 GeV SM Higgs boson signal is shown added to the background. Right: Fraction of events in the 0-jet category as a function of jet p_T threshold for 5 exclusive ranges of the number of primary vertices.

We select events in which the most (2nd most) energetic lepton has $p_T > 20$ (10) GeV and typically $E_T^{\text{miss}} > 20$ GeV. Estimation of SM backgrounds makes use of data control samples complemented by MC samples to extrapolate into the signal region. Upper limits are derived for the product of the Higgs boson production cross section and the $H \rightarrow WW$ branching fraction, $\sigma_H \times \text{BR}(H \rightarrow WW)$, relative to the SM Higgs expectation, $\sigma/\sigma_{\text{SM}}$. Combining all classes from 2011 and 2012 data, we obtain the 95% observed and median expected C.L. upper limits shown in Figure 11 (left). An excess of events is observed for low Higgs boson masses. Due to the poor mass resolution of this channel the excess extends over a large mass range. The significance of the excess at mass 125 GeV with respect to the background only hypothesis is 4.0 standard deviations for the combination of the 7 and 8 TeV data. The observed $\sigma/\sigma_{\text{SM}}$ value for $m_H = 125$ GeV is 0.76 ± 0.13 (stat.) ± 0.16 (syst.). A more complete account of the results in this channel can be found in [40].

3.4 Decay mode $H \rightarrow \tau\tau$

Under the assumption that its coupling is proportional to mass, we search for decays of this new particle to the heaviest accessible fermions – namely pairs of τ leptons and b quarks. The detection of τ leptons is challenging because they have a multitude of decay modes to leptons ($\tau \rightarrow l\nu\nu$, $l = e, \mu$), or to one or three π^\pm , possibly accompanied by π^0 's, and a ν_τ . CMS reconstructs the leptonic decays and several classes of hadronic decays with good efficiency and low fake rates as verified with $Z \rightarrow \tau\tau$ data [41].

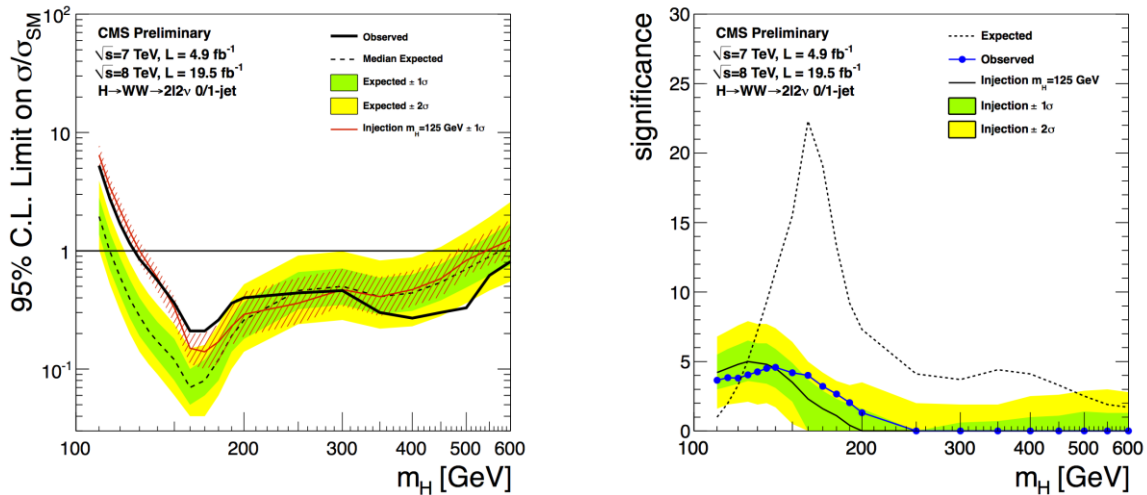


Figure 11. Left: Expected and observed 95% CL upper limits on the cross section times branching fraction, relative to the SM Higgs expectation, using the 7 and 8 TeV data. The expected limits in the presence of the Higgs with $m_H = 125$ GeV and its associated uncertainty are also shown (red). Right: The dashed line shows the significance expected for the search for a Higgs boson with a mass m_H if a Higgs boson of this mass exists. The solid line and colored bands show the expected significance at a mass m_H if the true Higgs boson mass is 125 GeV. The dots show the observed significance of the excess for the search for a Higgs boson with a mass m_H .

The challenge here is the understanding of the backgrounds. They are mostly extracted using control samples in data. Events are classified by five pairings ($\tau\tau\mu\mu$, $\tau\tau e e$, $\tau\mu\tau\mu$, $\tau\mu e e$, $\tau e\tau e$) of tau decays and by the presence of jets. The classification by the number of additional jets in the final state is used to enhance the contribution of different Higgs boson production mechanisms.

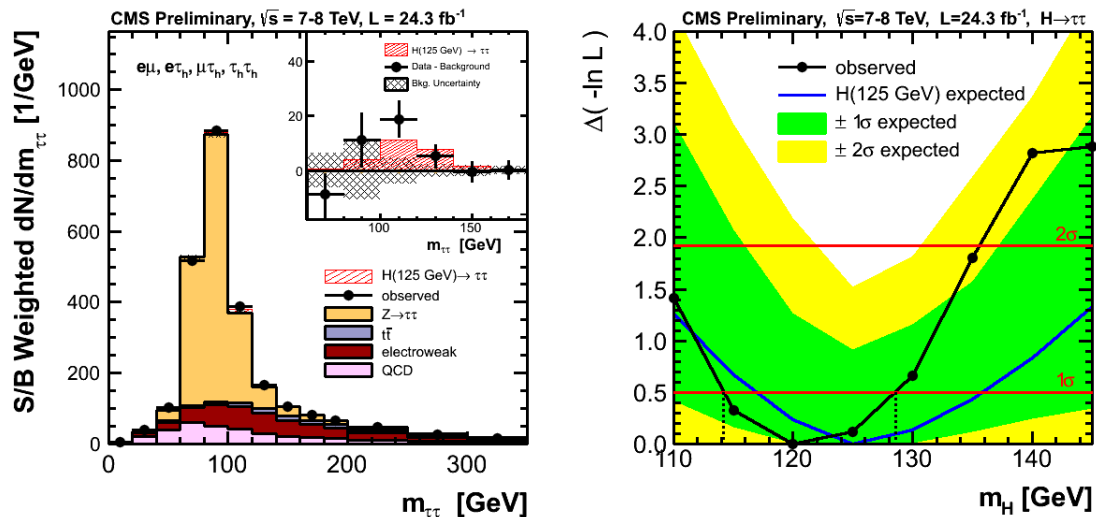


Figure 12. Left: Combined observed and expected $m_{\tau\tau}$ distributions for the $\mu\tau\tau$, $e\tau\tau$, $e\mu$ and $\tau\tau\tau\tau$ channels. The distributions obtained in each category of each channel are weighted by the ratio between the expected signal and background yields in the category. The insert shows the corresponding difference between the observed data and expected background distributions, together with the expected signal distribution for a standard-model Higgs signal at $m_H = 125$ GeV, with a focus on the signal region. Right: Log likelihood versus SM Higgs boson mass, combining all search channels. The black curve shows the result from the observed spectrum of tau pair invariant mass, and

the blue curve shows the result expected if the observed spectrum was equal to that expected from the background plus a SM Higgs boson signal at a mass of 125 GeV.

The one-jet category selects primarily signal events with a Higgs boson produced by gluon fusion, or in association with a W or Z boson decaying hadronically. Events in the vector-boson fusion (VBF) category are required to have two jets separated by a large rapidity gap, which mainly selects signal events with a Higgs boson produced by vector-boson fusion and strongly enhances the signal contribution. Different categories of events have different backgrounds and signal sensitivities. In each channel, the signal is separated from the background, and in particular from the irreducible $Z \rightarrow \tau\tau$, using the τ -pair mass reconstructed from the four-momenta of the visible decay products of the two τ leptons and from the missing transverse energy. The presence of neutrinos implies that the signal would appear as a broad enhancement over background.

Figure 12 (left) shows the observed and expected $m_{\tau\tau}$ distributions combined for different channels. An excess of events is seen in the mass region where a standard-model Higgs signal at $m_H = 125$ GeV is expected. The best-fit value for the signal strength combining all channels is $\mu = 1.1 \pm 0.4$ at $m_H = 125$ GeV. The minimum p-value of the excess is observed at $m_H = 120$ GeV, corresponding to a significance of 2.9 standard deviations. This is an indication that the new boson discovered in 2012 couples to τ leptons, with a strength compatible to the one predicted by the standard model. Figure 12 (right) shows the fit likelihood as a function of the Higgs mass. The best fit is obtained for a SM Higgs boson of $m_H = 120^{+9.7}_{-7}$ (stat+syst) GeV. A more complete account of the results in this channel can be found in [42].

3.5 Decay mode $H \rightarrow b\bar{b}$

A search for the standard model Higgs boson H decaying to $b\bar{b}$ when produced in association with a weak vector boson (V) was performed for the following modes: $W(\mu\nu)H$, $W(e\nu)H$, $Z(\mu\mu)H$, $Z(ee)H$ and $Z(\nu\nu)H$ [43]. The search was performed in data samples corresponding to integrated luminosities of 5.0 fb^{-1} at $\sqrt{s} = 7$ TeV and 12.1 fb^{-1} at $\sqrt{s} = 8$ TeV, recorded by the CMS experiment at the LHC.

Upper limits, at 95% confidence level, on the VH production cross section times the $H \rightarrow b\bar{b}$ branching ratio, with respect to the expectations for a standard model Higgs boson, were derived for a Higgs boson in the mass range 110–135 GeV. In this range, the observed upper limits vary from 1.0 to 4.2 times the standard model prediction; the corresponding expected limits vary from 0.9 to 1.9. An excess of events is observed above the expected background with a local significance of 2.2 standard deviations, which is consistent with the expectation from the production of the standard model Higgs boson.

4. Conclusions

The CMS experiment is traversing an historic period in particle physics following the discovery of a new boson in 2012. The investigation of the nature of this new particle is being intensively pursued. Improved measurements of the strength of the interaction of this particle with other particles together with comparisons of data with expectations of a variety of spin-parity models, reported here, strongly indicate that indeed we have observed a Higgs boson that is responsible for Electroweak Symmetry Breaking.

References

1. L. Evans, P. Bryant (editors), *LHC Machine*, JINST 03 (2008) S08001, doi:10.1088/1748-0221/3/08/S08001
2. CMS Collaboration, *Observation of a new boson at a mass of 125 GeV with the CMS experiment at the LHC*, Phys. Lett. B 716 (2012) 30–61, doi:10.1016/j.physletb.2012.08.021, arXiv:1207.7235.

3. ATLAS Collaboration, *Observation of a new particle in the search for the Standard Model Higgs boson with the ATLAS detector at the LHC*, Phys.Lett.B 716 (2012) 1-29.
4. CMS Collaboration, *The CMS experiment at the CERN LHC*, JINST 03 (2008) S08004, doi:10.1088/1748-0221/3/08/S08004.
5. J.R. Ellis, M.K. Gaillard, D.V. Nanopoulos, *A phenomenological profile of the Higgs boson*, Nucl. Phys. B 106 (1976) 292, doi:10.1016/0550-3213(76)90382-5.
6. H.M. Georgi, S.L. Glashow, M.E. Machacek, D.V. Nanopoulos, *Higgs Bosons from Two Gluon Annihilation in Proton Proton Collisions*, Phys. Rev. Lett. 40 (1978) 692, doi:10.1103/PhysRevLett.40.692.
7. S.L. Glashow, D.V. Nanopoulos, A. Yildiz, *Associated Production of Higgs Bosons and Z Particles*, Phys. Rev. D 18 (1978) 1724, doi:10.1103/PhysRevD.18.1724.
8. S. Alioli, P. Nason, C. Oleari, E. Re, *NLO Higgs boson production via gluon fusion matched with shower in POWHEG*, JHEP 04 (2009) 002, doi:10.1088/1126-6708/2009/04/002.
9. P. Nason, C. Oleari, *NLO Higgs boson production via vector boson fusion matched with shower in POWHEG*, JHEP 02 (2010) 037, doi:10.1007/JHEP02(2010)037.
10. T. Sjöstrand, S. Mrenna, P.Z. Skands, *PYTHIA 6.4 physics and manual*, JHEP 05 (2006) 026, doi:10.1088/1126-6708/2006/05/026.
11. S. Gieseke, D. Grellscheid, K. Hamilton, A. Ribon, P. Richardson, et al., *Herwig++ 2.0 Release Note (2006)*, arXiv:hep-ph/0609306.
12. J. Alwall, P. Demin, S. de Visscher, R. Frederix, M. Herquet, et al., *MadGraph/MadEvent v4: the new web generation*, JHEP 09 (2007) 028, doi:10.1088/1126-6708/2007/09/028, arXiv:0706.2334.
13. S. Agostinelli, et al., *GEANT4—a simulation toolkit*, Nucl. Instrum. Meth. A 506 (2003) 250, doi:10.1016/S0168-9002(03)01368-8.
14. S. Actis et al., Nucl. Phys. B 811 (2009) 182, doi:10.1016/j.nuclphysb.2008.11.024, arXiv:0809.3667.
15. CMS Collaboration, *Updated measurements of the Higgs boson at 125 GeV in the two photon decay channel*, CMS PAS HIG-13-001, CDS Record 1530524 (2013).
16. H. B. Prosper, *Multivariate methods in particle physics: Today and tomorrow*, 2008, PoS ACAT08 (2008) 010.
17. P. C. Bhat, *Multivariate Analysis Methods in Particle Physics*, Ann. Rev. Nucl. Part. Sci. 61 (2011) 281-309.
18. S. Alioli et al., *NLO Higgs boson production via gluon fusion matched with shower in POWHEG*, JHEP 04 (2009) 002, doi:10.1088/1126-6708/2009/04/002.
19. P. Nason and C. Oleari, *NLO Higgs boson production via vector-boson fusion matched with shower in POWHEG*, JHEP 02 (2010) 037, doi:10.1007/JHEP02(2010)037.
20. T. Sjostrand, S. Mrenna, and P. Z. Skands, *PYTHIA 6.4 Physics and Manual*, JHEP 0605 (2006) 026, doi:10.1088/1126-6708/2006/05/026.
21. G. Bozzi et al., *The $q(T)$ spectrum of the Higgs boson at the LHC in QCD perturbation theory*, Phys. Lett. B 564 (2003) 65, doi:10.1016/S0370-2693(03)00656-7.
22. G. Bozzi et al., *Transverse-momentum resummation and the spectrum of the Higgs boson at the LHC*, Nucl. Phys. B 737 (2006) 73, doi:10.1016/j.nuclphysb.2005.12.022.
23. LHC Higgs Cross Section Working Group Collaboration, *Handbook of LHC Higgs Cross Sections: 1. Inclusive Observables*, CERN Report CERN-2011-002, (2011).
24. CMS Collaboration, *Evidence for a new state decaying into two photons in the search for the standard model Higgs boson in pp collisions*, CDS Record 1460419 (2012).
25. CMS Collaboration, *Study of the Mass and Spin-Parity of the Higgs Boson Candidate via Its Decays to Z Boson Pairs*, Phys. Rev. Lett. 110 (2013) 081803, doi:10.1103/PhysRevLett.110.081803, arXiv:1212.6639.
26. S. Frixione, P. Nason, and C. Oleari, *Matching NLO QCD computations with Parton Shower simulations: the POWHEG method*, JHEP 11 (2007) 070, doi:10.1088/1126-6708/2007/11/070, arXiv:0709.2092.
27. Y. Gao et al., *Spin determination of single-produced resonances at hadron colliders*, Phys. Rev. D 81 (2010) 075022, doi:10.1103/PhysRevD.81.075022, arXiv:1001.3396.

28. G. Passarino, C. Sturm, and S. Uccirati, *Higgs Pseudo-Observables, Second Riemann Sheet and All That*, Nucl. Phys. B 834 (2010) 77, doi:10.1016/j.nuclphysb.2010.03.013, arXiv:1001.3360.
29. S. Gorla, G. Passarino, and D. Rosco, *The Higgs Boson Lineshape*, Nucl. Phys. B 864 (2012) 530–579, doi:10.1016/j.nuclphysb.2012.07.006, arXiv:1112.5517.
30. N. Kauer and G. Passarino, *Inadequacy of zero-width approximation for a light Higgs boson signal*, JHEP 1208 (2012) 116, doi:10.1007/JHEP08(2012)116, arXiv:1206.4803.
31. CMS Collaboration, *Properties of the Higgs-like boson in the decay H to ZZ to $4l$ in pp collisions at $\sqrt{s} = 7$ and 8 TeV*, CMS PAS HIG-13-002, CDS Record 1523767 (2013).
32. J. Alwall et al., *MadGraph/MadEvent v4: The NewWeb Generation*, JHEP 09 (2007) 028, doi:10.1088/1126-6708/2007/09/028, arXiv:0706.2334.
33. T. Binoth, N. Kauer, and P. Mertsch, *Gluon-induced QCD corrections to $pp \rightarrow ZZ \rightarrow llll$* , in Proceedings of the XVI Int. Workshop on Deep-Inelastic Scattering and Related Topics (DIS'07). 2008. arXiv:0807.0024. doi:10.3360/dis.2008.142.
34. S. Bolognesi et al., *On the spin and parity of a single-produced resonance at the LHC*, Phys. Rev. D 86 (2012) 095031, doi:10.1103/PhysRevD.86.095031, arXiv:1208.4018.
35. Y. Chen, N. Tran, and R. Vega-Morales, *Scrutinizing the Higgs Signal and Background in the $2e2\mu$ Golden Channel*, arXiv:1211.1959.
36. J. M. Campbell and R. K. Ellis, *MCFM for the Tevatron and the LHC*, Nucl. Phys. Proc. Suppl. 205 (2010) 10, doi:10.1016/j.nuclphysbps.2010.08.011, arXiv:1007.3492.
37. J. M. Campbell and R. K. Ellis, *An update on vector boson pair production at hadron colliders*, Phys. Rev. D 60 (1999) 113006, doi:10.1103/PhysRevD.60.113006, arXiv:hep-ph/9905386.
38. J. M. Campbell, R. Ellis, and C. Williams, *Vector boson pair production at the LHC*, JHEP 07 (2011) 018, doi:10.1007/JHEP07(2011)018, arXiv:1105.0020.
39. P. Avery et al., *Precision studies of the Higgs boson decay channel $H \rightarrow ZZ^* \rightarrow 4l$ with MEKD*, accepted by Phys.Rev.D. (2012) arXiv:1210.0896.
40. CMS Collaboration, *Evidence for a particle decaying to $W+W^-$ in the fully leptonic final state in a standard model Higgs boson search in pp collisions at the LHC*, CMS PAS HIG-13-003, CDS Record 1523673 (2013).
41. CMS Collaboration, *Z inclusive cross-section via decays to tau pairs at 7 TeV*, JHEP 08 (2011) 117, doi:10.1007/JHEP08(2011)117, arXiv:1104.1617.
42. CMS Collaboration, *Search for the Standard-Model Higgs boson decaying to tau pairs in proton-proton collisions at $\sqrt{s} = 7$ and 8 TeV*, CMS PAS HIG-13-004, CDS Record 1528271 (2013).
43. CMS Collaboration, *Search for the standard model Higgs boson produced in association with W or Z bosons, and decaying to bottom quarks for HCP 2012*, CMS PAS HIG-12-044, CDS Record 1493618 (2012).